

Synthesis and Anti-Chikungunya Virus (CHIKV) Activity of Novel 1,4-Naphthoquinone Sulfonamide and Sulfonate Ester Derivatives

Paulo A. F. Pacheco,^a Daniel T. Gonzaga,^b Cláudio C. Cirne-Santos,^c Caroline S. Barros,^c Max W. L. Gomes,^c Rafaela S. P. Gomes,^c Mariana C. Gonçalves,^b Vitor F. Ferreira,^a Vitor W. Rabelo,^c Paula A. Abreu,^d Robson X. Faria,^e Gabriel O. de Resende,^f David R. da Rocha,^a Izabel C. N. P. Paixão^{*,c} and Fernando C. da Silva^{*,a}

^aDepartamento de Química Orgânica, Instituto de Química, Universidade Federal Fluminense, Campus do Valonguinho, 24020-141 Niterói-RJ, Brazil

^bUnidade de Farmácia (UFAR), Fundação Centro Universitário da Zona Oeste, 23070-200 Rio de Janeiro-RJ, Brazil

^cPrograma de Pós-Graduação em Ciências e Biotecnologia, Laboratório de Virologia Molecular e Biotecnologia Marinha, Departamento de Biologia Celular e Molecular, Instituto de Biologia, Universidade Federal Fluminense, 24020-141 Niterói-RJ, Brazil

^dInstituto de Biodiversidade e Sustentabilidade, Universidade Federal do Rio de Janeiro, 27965-045 Macaé-RJ, Brazil

^eLaboratório de Avaliação e Promoção da Saúde Ambiental, Fundação Oswaldo Cruz, Pavilhão Lauro Travassos, Instituto Oswaldo Cruz, Manguinhos, 21045-900 Rio de Janeiro-RJ, Brazil

^fInstituto Federal de Educação, Ciência e Tecnologia do Rio de Janeiro, Unidade Maracanã, 20270-021 Rio de Janeiro-RJ, Brazil

Chikungunya virus (CHIKV) is a re-emerging disease caused by an alphavirus of the *Togaviridae* family. Since its first description in 1952, the disease has spread worldwide, affecting populations in both tropical and temperate countries. To date, there is no licensed vaccine or specific pharmacological treatment. Therefore, there is an increasing urgency in developing new antiviral drugs capable of specifically inhibiting viral replication. In the present work, we report the synthesis and antiviral activity evaluation of nineteen naphthoquinone derivatives, containing a sulfonamide or sulfonate group. Cell viability assays indicated a low toxic potential for all tested compounds and inhibitory assays against CHIKV identified five compounds with potent activity. The compounds were also evaluated for their virucidal potential, and the results demonstrated that compound **11a** exhibited a virucidal effect higher than 70% in the treatment with 20 μ M. Furthermore, *in silico* studies were performed to predict the antiviral drug targets.

Keywords: Chikungunya virus, naphthoquinone, sulfonamide, sulfonate

Introduction

Quinones constitute a class of natural products with wide distribution in nature and are structurally characterized by two conjugated carbonyl groups in six-membered unsaturated rings.¹ Naphthoquinone presents

an aromatic ring fused to the quinonoid nucleus, and this chemical characteristic is identified as responsible for its redox potential.² Naphthoquinones are considered privileged structures in Medicinal Chemistry and have been extensively studied as synthetic platforms due to their broad range of biological properties, such as anticancer, antibacterial, anti-inflammatory, antiviral, and others.³⁻⁹

Chikungunya virus (CHIKV) is a mosquito-transmitted alphavirus of the *Togaviridae* family that causes a febrile

*e-mail: izabeluff@gmail.com; fcsilva@id.uff.br

Editor handled this article: Brenno A. D. Neto (Associate)

syndrome (Chikungunya fever) usually associated with intense and debilitating arthralgia.¹⁰⁻¹² It was first described in 1952 during an outbreak in southern Tanzania.¹³ Since then, it has spread, and infection cases have been reported in all continents, except Antarctica and approximately 3-5 million cases of CHIKV are reported each year worldwide.¹⁴ The disease is transmitted during blood repast of peridomestic mosquitoes, such as *Aedes aegypti* and *Aedes albopictus*.^{15,16}

Although research has brought compounds with activity against CHIKV, most of them have not yet been validated *in vivo* and in clinical trials. Thus, until now, neither specific antiviral drugs nor a licensed vaccine are available. Chikungunya fever therapy is based on supportive measures and the treatment of symptoms through non-steroidal anti-inflammatory drugs (NSAIDs) and fluid therapy.¹⁷ This shows that the effort to find a specific treatment is extremely important. The sulfonamide group ($-\text{SO}_2\text{NH}_2$) is found in the structure of several drugs with high clinical relevance, such as sulfamethoxazole (**1**, antibacterial), acetazolamide (**2**, carbonic anhydrase inhibitors), celecoxib (**3**, cyclooxygenase-2 inhibitor), and glibenclamide (**4**, hypoglycemic agent) (Figure 1).^{7,18-20} Other biological activities have also been reported by compounds containing this functionality, such as anticancer, antimicrobial, anti-inflammatory, antioxidant, and others.²¹⁻²⁴ Regarding antiviral activity, sulfonamide moiety is present in the compound structure used clinically to treat viral infections, such as amprevir (**5**) and darunavir (**6**).^{25,26}

Herein, we describe the synthesis of two series of naphthoquinones derivatives containing a sulfonamide group (**8a-8e**, **9a-9e**, and **10a-10d**) and sulfonate esters

group (**11a-11e**). Additionally, all synthesized compounds were also screened *in vitro* for their cytotoxicity and anti-CHIKV activity.

Experimental

Chemistry

Materials and methods

The solvents and reagents were obtained from Merck (São Paulo, Brazil) and used without further purification. For qualitative monitoring of the reaction progress, analytical thin-layer chromatography (TLC) was produced with silica gel plates (Merck, São Paulo, Brazil, TLC silica gel 60 F254), and the plots were visualized using UV light (Sigma-Aldrich, São Paulo, Brazil). For purification of the final compounds, column chromatography was performed with silica gel 60 (Merck 70-230 mesh, São Paulo, Brazil). Melting points, when necessary, were obtained on a Thermo Scientific 9100 apparatus (Waltham, USA) and were uncorrected. All final products were submitted to complete spectroscopic characterization. Infrared spectra were measured with KBr pellets on a PerkinElmer model 1420 Fourier transform infrared (FTIR) spectrophotometer (São Paulo, Brazil), and the spectra were calibrated using the 1601.8 cm^{-1} polystyrene absorbances. Nuclear magnetic resonance (NMR) spectra were obtained with a Varian Unity Plus VXR 500 MHz (Palo Alto, USA) instrument in dimethyl sulfoxide ($\text{DMSO}-d_6$) solutions. The chemical shift data were reported in units of δ (ppm) downfield from tetramethylsilane (TMS) or the solvent, either of which was used as an internal standard, coupling constants (J) are reported in hertz and refer to apparent peak multiplicities. High-resolution mass spectra

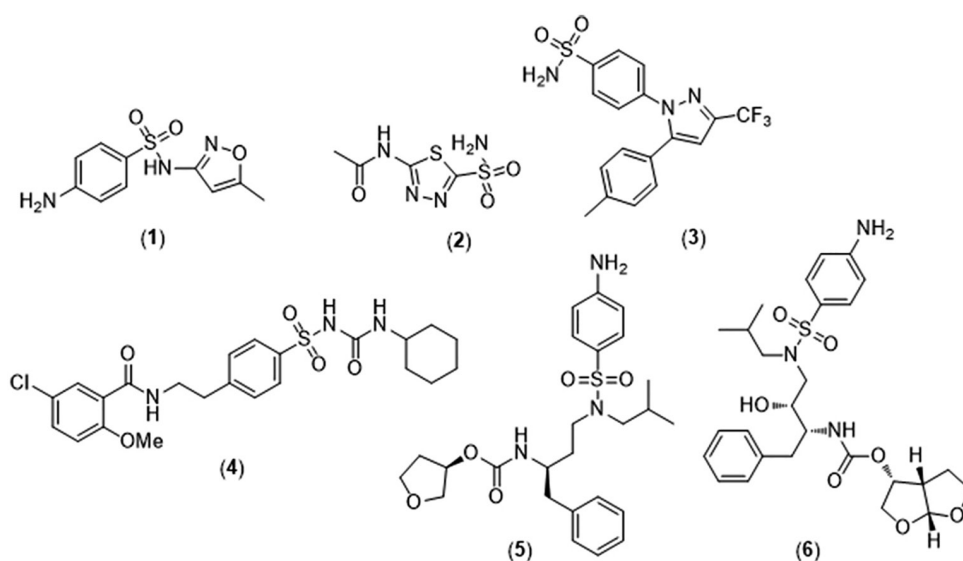


Figure 1. Commercial drugs containing a sulfonamide moiety.

(HRMS) were recorded on a MICROMASS Q-TOF mass spectrometer (Waters, Milford, USA).

General procedure for **8a-8e**, **9a-9e**, and **10a-10d** preparation

The corresponding amino-naphthoquinone (**7a-7c**) (1 mmol) was dissolved with pyridine (4 mL) under magnetic stirring in a round-bottom flask. Next, 4-dimethylaminopyridine (DMAP) (0.1 mmol) and the appropriate sulfonyl chloride (1.5 mmol) were added to the reaction flask, and the mixture was stirred for 24 h at room temperature. After the start material total consumption, the aqueous solution of HCl 1 M was added to neutralize the medium, and the resulting mixture was extracted with ethyl acetate. The organic phase was washed successively with saturated NaHCO₃ solution, water, and brine, dried over sodium sulfate anhydrous, and evaporated under reduced pressure. The resulting crude product was purified in silicagel column chromatography using a gradient mixture of hexane/ethyl acetate as eluent to obtain the pure derivatives.

N-(4-((1,4-Dioxo-1,4-dihydronaphthalen-2-yl)amino)phenyl) benzenesulfonamide (**8a**)

Dark brown solid; yield > 99% (400 mg); mp 241-243 °C; IR (KBr) ν / cm⁻¹ 723, 831, 920, 1226, 1340, 1449, 1607, 1669, 3304; ¹H NMR (500 MHz, DMSO-*d*₆) δ 5.96 (s, 1H), 7.15 (d, 2H, *J* 8.8 Hz), 7.25 (d, 2H, *J* 8.8 Hz), 7.53-7.56 (m, 2H), 7.62-7.59 (m, 1H), 7.74-7.78 (m, 3H), 7.83 (td, 1H, *J* 1.3 and 7.5 Hz), 7.94 (dd, 1H, *J* 0.9 and 7.7 Hz), 8.03 (dd, 1H, *J* 0.9 and 7.7 Hz), 8.91 (s, 1H), 10.16 (s, 1H); ¹³C NMR (125 MHz attached proton test (APT), DMSO-*d*₆) δ 101.8, 121.1, 124.2, 125.0, 125.7, 126.4, 128.9, 130.2, 132.2, 132.4, 132.5, 134.1, 134.5, 134.6, 139.5, 145.9, 181.2, 182.1; HRESIMS *m/z*, calcd. for C₂₂H₁₅N₂O₄S⁻ [M - H]⁻: 403.0758, found: 403.0772.

N-(4-((1,4-Dioxo-1,4-dihydronaphthalen-2-yl)amino)phenyl)-4-methylbenzenesulfonamide (**8b**)

Dark brown solid; yield > 99% (414 mg); mp 227-229 °C; IR (KBr) ν / cm⁻¹ 724, 824, 920, 1157, 1226, 1340, 1530, 1607, 1670, 3121; ¹H NMR (500 MHz, DMSO-*d*₆) δ 2.35 (s, 3H), 5.95 (s, 1H), 7.15 (d, 2H, *J* 8.9 Hz), 7.24 (d, 2H, *J* 8.9 Hz), 7.34 (d, 2H, *J* 8.4 Hz), 7.66 (d, 2H, *J* 8.3 Hz), 7.75 (td, 1H, *J* 1.3 and 7.5 Hz), 7.83 (td, 1H, *J* 1.3 and 7.5 Hz), 7.94 (dd, 1H, *J* 1.0 and 7.6 Hz), 8.03 (dd, 1H, *J* 1.0 and 7.6 Hz), 8.91 (s, 1H), 10.09 (s, 1H); ¹³C NMR (125 MHz APT, DMSO-*d*₆) δ 20.6, 101.8, 121.0, 124.2, 125.0, 125.7, 126.4, 129.3, 130.2, 132.2, 132.5, 133.9, 134.5, 134.7, 136.7, 142.9, 145.9, 181.2, 182.1; HRESIMS *m/z*, calcd. for C₂₃H₁₈N₂NaO₄S⁺ [M + H]⁺: 441.0879, found: 441.0879.

N-(4-((1,4-Dioxo-1,4-dihydronaphthalen-2-yl)amino)phenyl) naphthalene-2-sulfonamide (**8c**)

Dark brown solid; yield > 99% (450 mg); mp 222-224 °C; IR (KBr) ν / cm⁻¹ 725, 822, 924, 1154, 1229, 1335, 1454, 1610, 1665, 3108; ¹H NMR (500 MHz, DMSO-*d*₆) δ 5.94 (s, 1H), 7.18-7.23 (m, 4H), 7.70-7.74 (m, 2H), 7.75 (td, 1H, *J* 1.3 and 7.6 Hz), 7.81-7.84 (m, 2H), 7.93 (dd, 1H, *J* 0.9 and 7.7 Hz), 7.99-8.03 (m, 2H), 8.07-8.11 (m, 2H), 8.42 (d, 1H, *J* 1.4 Hz), 8.88 (s, 1H), 10.29 (s, 1H); ¹³C NMR (125 MHz APT, DMSO-*d*₆) δ 101.7, 121.2, 121.8, 124.2, 124.9, 125.7, 127.3, 127.5, 128.5, 128.8, 129.0, 130.1, 131.4, 132.1, 132.4, 133.9, 134.0, 134.4, 134.8, 136.7, 145.8, 181.1, 182.0; HRESIMS *m/z*, calcd. for C₂₆H₁₇N₂O₄S⁻ [M - H]⁻: 453.0915, found: 453.0916.

N-(4-((1,4-Dioxo-1,4-dihydronaphthalen-2-yl)amino)phenyl)-4-fluorobenzenesulfonamide (**8d**)

Dark brown solid; yield > 99% (418 mg); mp 210-212 °C; IR (KBr) ν / cm⁻¹ 724, 829, 923, 1153, 1347, 1406, 1594, 1669, 3107; ¹H NMR (500 MHz, DMSO-*d*₆) δ 5.99 (s, 1H), 7.16 (d, 2H, *J* 8.8 Hz), 7.27 (d, 2H, *J* 8.8 Hz), 7.38 (t, 2H, *J* 8.8 Hz), 7.76 (td, 1H, *J* 1.3 and 7.5 Hz), 7.82-7.86 (m, 3H), 7.95 (dd, 1H, *J* 1.0 and 7.7 Hz), 8.04 (dd, 1H, *J* 1.1 and 7.7 Hz), 8.94 (s, 1H), 10.20 (s, 1H); ¹³C NMR (125 MHz APT, DMSO-*d*₆) δ 101.9, 116.1 (d, *J* 23.0 Hz), 124.2, 125.0, 125.7, 129.4 (d, *J* 10.0 Hz), 130.2, 132.2, 132.4, 134.3, 134.5, 135.8 (d, *J* 3.0 Hz), 145.9, 164.1 (d, *J* 245.0 Hz), 181.2, 182.2; HRESIMS *m/z*, calcd. for C₂₂H₁₅FN₂NaO₄S⁺ [M + Na]⁺: 445.0629, found: 445.0615.

N-(4-((1,4-Dioxo-1,4-dihydronaphthalen-2-yl)amino)phenyl)-4-nitrobenzenesulfonamide (**8e**)

Dark red solid; yield > 99% (445 mg); mp > d 210 °C; IR (KBr) ν / cm⁻¹ 740, 854, 1194, 1347, 1624, 1667, 3104; ¹H NMR (500 MHz, DMSO-*d*₆) δ 6.01 (s, 1H), 7.17 (d, 1H, *J* 8.8 Hz), 7.29 (d, 1H, *J* 8.8 Hz), 7.76 (td, *J* 1.4 and 7.5 Hz), 7.84 (td, 1H, *J* 1.4 and 7.5 Hz), 7.94 (ddd, 1H, *J* 0.4, 1.4 and 7.6 Hz), 8.01-8.05 (m, 2H), 8.37 (d, 2H, *J* 9.0 Hz), 8.95 (s, 1H), 10.50 (s, 1H); ¹³C NMR (125 MHz APT, DMSO-*d*₆) δ 102.0, 121.8, 124.2, 124.2, 125.7, 128.0, 130.2, 132.2, 132.4, 133.6, 134.5, 134.8, 144.9, 145.7, 149.7, 181.2, 182.1; HRESIMS *m/z*, calcd. for C₂₂H₁₄N₃O₆S⁻ [M - H]⁻: 448.0609, found: 448.0626.

N-(4-((3-Chloro-1,4-dioxo-1,4-dihydronaphthalen-2-yl)amino)phenyl)benzenesulfonamide (**9a**)

Orange solid; yield > 99% (434 mg); mp 239-241 °C; IR (KBr) ν / cm⁻¹ 750, 843, 914, 1155, 1296, 1331, 1465, 1634, 1677, 3248; ¹H NMR (500 MHz, DMSO-*d*₆) δ 7.01 (m, 4H), 7.51-7.55 (m, 2H), 7.59-7.61 (m, 1H), 7.73-7.75 (m, 2H), 7.78 (td, 1H, *J* 1.1 and 7.5 Hz), 7.85 (td, 1H, *J* 1.1

and 7.5 Hz), 8.00-8.03 (m, 2H), 9.01 (s, 1H), 10.02 (s, 1H); ^{13}C NMR (125 MHz APT, DMSO- d_6) δ 114.1, 120.7, 125.3, 126.3, 126.7, 126.9, 129.2, 130.2, 132.1, 133.1, 133.4, 134.3, 135.0, 135.5, 139.5, 143.4, 176.9, 180.2; HRESIMS m/z , calcd. for $\text{C}_{22}\text{H}_{15}\text{ClN}_2\text{NaO}_4\text{S}^+ [\text{M} + \text{Na}]^+$: 461.0333, found: 461.0312.

N-(4-((3-Chloro-1,4-dioxo-1,4-dihydronaphthalen-2-yl) amino)phenyl)-4-methylbenzenesulfonamide (**9b**)

Deep red solid; yield > 99% (448 mg); mp 172-174 °C; IR (KBr) ν / cm^{-1} 738, 809, 915, 1157, 1220, 1329, 1491, 1640, 1673, 3231; ^1H NMR (500 MHz, DMSO- d_6) δ 2.35 (s, 3H), 7.03 (s, 4H), 7.33 (d, J 8.0 Hz), 7.62 (d, J 8.3 Hz), 7.78 (td, 1H, J 1.3 and 7.5 Hz), 7.85 (td, 1H, J 1.2 and 7.5 Hz), 8.00-8.03 (m, 2H), 9.01 (s, 1H), 9.96 (s, 1H); ^{13}C NMR (125 MHz APT, DMSO- d_6) δ 20.7, 113.7, 120.3, 124.8, 125.9, 126.3, 126.5, 129.3, 130.0, 131.8, 132.9, 134.3, 134.6, 135.1, 136.6, 142.9, 143.0, 176.3, 179.7; HRESIMS m/z , calcd. for $\text{C}_{23}\text{H}_{17}\text{ClN}_2\text{NaO}_4\text{S}^+ [\text{M} + \text{Na}]^+$: 475.0490, found: 475.0479.

N-(4-((3-Chloro-1,4-dioxo-1,4-dihydronaphthalen-2-yl) amino)phenyl)naphthalene-2-sulfonamide (**9c**)

Dark red solid; yield > 99% (484 mg); mp 211-213 °C; IR (KBr) ν / cm^{-1} 751, 822, 913, 1155, 1291, 1332, 1494, 1636, 1674, 3234; ^1H NMR (500 MHz, DMSO- d_6) δ 6.97 (d, 2H, J 8.8 Hz), 7.05 (d, 2H, J 8.8 Hz), 7.62-7.70 (m, 2H), 7.75-7.79 (m, 2H), 7.84 (td, 1H, J 1.3 and 7.5 Hz), 7.98-8.01 (m, 3H), 8.06-8.09 (m, 2H), 8.37 (d, 1H, J 1.5 Hz), 8.98 (s, 1H), 10.13 (s, 1H); ^{13}C NMR (125 MHz APT, DMSO- d_6) δ 113.7, 121.9, 124.7, 125.8, 126.1, 127.3, 127.5, 127.6, 128.5, 128.9, 128.9, 129.9, 131.3, 131.7, 132.8, 134.0, 134.5, 135.2, 136.5, 142.9, 176.2, 179.7; HRESIMS m/z , $[\text{M} - \text{H}]^-$ calcd. for $\text{C}_{26}\text{H}_{16}\text{ClN}_2\text{O}_4\text{S}^-$: 487.0525, found: 487.0526.

N-(4-((3-Chloro-1,4-dioxo-1,4-dihydronaphthalen-2-yl) amino)phenyl)-4-fluorobenzenesulfonamide (**9d**)

Brown solid; yield > 99% (452 mg); mp 173-175 °C; IR (KBr) ν / cm^{-1} 790, 838, 916, 1165, 1236, 1379, 1430, 1669, 3246; ^1H NMR (500 MHz, DMSO- d_6) δ 7.00-7.03 (m, 4H), 7.33-7.38 (m, 2H), 7.76-7.80 (m, 3H), 7.85 (td, 1H, J 1.1 and 7.7 Hz), 8.02 (dd, 1H, J 1.1 and 7.7 Hz), 9.02 (s, 1H), 10.04 (s, 1H); ^{13}C NMR (125 MHz APT, DMSO- d_6) δ 113.8, 115.9 (d, J 22.7 Hz), 120.5, 124.8, 125.8, 126.2, 129.5 (d, J 10.0 Hz), 129.9, 131.8, 132.8, 133.8, 134.5, 135.4, 135.7 (d, J 3.0 Hz), 142.9, 164.0 (d, J 253.0 Hz), 176.2, 179.7; HRESIMS m/z , calcd. for $\text{C}_{22}\text{H}_{14}\text{ClFN}_2\text{NaO}_4\text{S}^+ [\text{M} + \text{Na}]^+$: 479.0239, found: 479.0220.

N-(4-((3-Chloro-1,4-dioxo-1,4-dihydronaphthalen-2-yl) amino)phenyl)-4-nitrobenzenesulfonamide (**9e**)

Yield > 99% (479 mg); deep brown solid; mp 223-225 °C; IR (KBr) ν / cm^{-1} 737, 847, 1159, 1257, 1379, 1491, 1598, 1699, 2918, 3103, 3239; ^1H NMR (500 MHz, DMSO- d_6) δ 7.03 (s, 4H), 7.79 (td, 1H, J 1.3 and 7.5 Hz), 7.85 (td, 1H, J 1.3 and 7.5 Hz), 7.98 (d, 2H, J 8.9 Hz), 8.01-8.03 (m, 2H), 8.36 (d, 2H, J 8.9 Hz), 9.04 (s, 1H), 10.36 (s, 1H); ^{13}C NMR (125 MHz APT, DMSO- d_6) δ 114.3, 121.0, 124.1, 124.7, 125.8, 126.2, 128.1, 130.0, 131.7, 132.8, 133.0, 134.5, 135.9, 142.8, 144.8, 149.6, 176.3, 179.6; HRESIMS m/z , calcd. for $\text{C}_{22}\text{H}_{13}\text{ClN}_3\text{O}_6\text{S}^+ [\text{M} - \text{H}]^+$: 482.0219, found: 482.0229.

N-(3-((3-Chloro-1,4-dioxo-1,4-dihydronaphthalen-2-yl) amino)phenyl)benzenesulfonamide (**10a**)

Yield 55% (241 mg); deep brown solid; mp 244-246 °C; IR (KBr) ν / cm^{-1} 726, 842, 1330, 1638, 1677, 3244; ^1H NMR (500 MHz, DMSO- d_6) δ 10.13 (s, 1H), 9.09 (s, 1H), 8.04 (dd, 1H, J 1.5 and 8.0 Hz), 8.01 (dd, 1H, J 1.5 and 8.0 Hz), 7.86 (td, 1H, J 1.4 and 7.5 Hz), 7.76-7.82 (m, 3H), 7.58-7.61 (m, 1H), 7.51-7.54 (m, 2H), 7.14 (t, 1H, J 8.0 Hz), 6.87-6.90 (m, 2H), 6.80-6.82 (m, 1H); ^{13}C NMR (125 MHz APT, DMSO- d_6) δ 115.0, 115.5, 116.0, 119.6, 125.8, 126.2, 126.3, 128.2, 128.8, 130.0, 131.6, 132.5, 132.9, 134.4, 137.4, 139.5, 139.6, 142.9, 176.3, 179.6; HRESIMS m/z , calcd. for $\text{C}_{22}\text{H}_{15}\text{ClN}_2\text{NaO}_4\text{S}^+ [\text{M} + \text{Na}]^+$: 461.0333, found 461.0334.

N-(3-((3-Chloro-1,4-dioxo-1,4-dihydronaphthalen-2-yl) amino)phenyl)-4-methylbenzenesulfonamide (**10b**)

Yield 77% (348 mg); red solid; mp 137-139 °C; IR (KBr) ν / cm^{-1} 717, 842, 1153, 1330, 1646, 1673, 3286; ^1H NMR (500 MHz, DMSO- d_6) δ 10.05 (s, 1H), 9.08 (s, 1H), 8.04 (dd, 1H, J 0.5 and 7.5 Hz), 8.02 (dd, 1H, J 0.5 and 7.5 Hz), 7.87 (td, 1H, J 1.5 and 7.5 Hz), 7.86 (td, 1H, J 1.5 and 7.5 Hz), 7.65 (d, 2H, J 8.5 Hz), 7.32 (d, 2H, J 8.5 Hz), 7.14 (t, 1H, J 8.0 Hz), 6.88-6.87 (m, 2H), 6.81-6.80 (m, 1H), 2.33 (s, 3H); ^{13}C NMR (125 MHz APT, DMSO- d_6) δ 20.6, 115.0, 115.4, 115.9, 119.5, 125.8, 126.2, 128.2, 126.4, 129.2, 130.0, 131.6, 132.9, 134.4, 136.8, 137.5, 139.5, 142.8, 142.9, 176.3, 179.6; HRESIMS m/z , calcd. for $\text{C}_{23}\text{H}_{17}\text{ClN}_2\text{NaO}_4\text{S}^+ [\text{M} + \text{Na}]^+$: 475.0490, found 475.0461.

N-(3-((3-Chloro-1,4-dioxo-1,4-dihydronaphthalen-2-yl) amino)phenyl)naphthalene-2-sulfonamide (**10c**)

Yield 70% (342 mg); deep brown solid; mp 240-242 °C; IR (KBr) ν / cm^{-1} 748, 844, 1151, 1330, 1593, 1675, 3213; ^1H NMR (500 MHz, DMSO- d_6) δ 6.77-6.79 (m, 1H), 6.90-6.92 (m, 1H), 6.94-6.95 (m, 1H), 7.12 (t, 1H,

7.80 Hz), 7.62-7.65 (m, 1H), 7.66-7.70 (m, 1H), 7.77-7.81 (m, 2H), 7.86 (td, 1H, *J* 1.4 and 7.5 Hz), 7.97-8.00 (m, 2H), 8.03 (dd, 1H, *J* 1.0 and 7.6 Hz), 8.05-8.07 (m, 2H), 8.41 (d, 1H, *J* 1.5 Hz), 9.06 (s, 1H), 10.22 (s, 1H); ¹³C NMR (125 MHz APT, DMSO-*d*₆) δ 115.0, 115.6, 116.0, 119.6, 121.8, 125.8, 126.2, 127.0, 127.5, 127.6, 128.2, 128.5, 128.8, 129.0, 130.0, 131.3, 131.6, 132.9, 134.0, 134.4, 136.6, 137.4, 139.5, 142.9, 176.3, 179.5; HRESIMS *m/z*, calcd. for C₂₆H₁₇ClN₂NaO₄S⁺ [M + Na]⁺: 511.0490, found: 511.0495.

N-(3-((3-Chloro-1,4-dioxo-1,4-dihydronaphthalen-2-yl) amino)phenyl)-4-nitrobenzenesulfonamide (**10d**)

Yield 45% (218 mg); brown solid; mp 204-206 °C; IR (KBr) ν / cm⁻¹ 734, 850, 1154, 1343, 1594, 1676, 3182; ¹H NMR (500 MHz, DMSO-*d*₆) δ 6.86-6.88 (m, 2H), 6.89-6.91 (m, 1H), 7.19 (t, 1H, *J* 8.0 Hz), 7.80 (td, 1H, *J* 1.5 and 7.5 Hz), 7.87 (td, 1H, *J* 1.5 and 7.5 Hz), 8.00 (s, 4H), 8.35 (d, 2H, *J* 9.0 Hz), 9.10 (s, 1H), 10.47 (s, 1H); ¹³C NMR (125 MHz APT, DMSO-*d*₆) δ 115.1, 115.9, 116.5, 120.1, 124.2, 125.8, 126.2, 128.0, 128.4, 130.0, 131.6, 132.9, 134.4, 136.5, 139.6, 142.9, 144.9, 149.7, 176.3, 179.6; HRESIMS *m/z*, calcd. for C₂₂H₁₄ClN₃NaO₆S⁺ [M + Na]⁺: 506.0184, found: 506.0152.

General procedure for **11a-11e** preparation

A stirred solution of **7d** (100 mg; 0.540 mmol) in 5 mL of acetonitrile was cooled in an ice bath, and 2.16 mmol of the appropriate sulfonyl chloride was added. Subsequently, trimethylamine (1.6 mmol) was added to the reaction mixture, and the ice bath was removed. The reaction occurred at room temperature for an additional 1 h. After the starting material total consumption, the reaction mixture was poured into 25 mL of water and extracted using ethyl acetate (3 × 50 mL). The organic phase was washed with brine (3 × 50 mL), dried with anhydrous sodium sulfate, filtered, and evaporated under reduced pressure. The mixture was purified by column chromatography on silicagel using a gradient mixture of hexane/ethyl acetate as eluent to obtain the pure derivatives.

7-Amino-5,8-dioxo-5,8-dihydronaphthalen-1-ylbenzenesulfonate (**11a**)

Orange solid; yield 95% (169 mg); mp 216-217 °C; IR (KBr) ν / cm⁻¹ 694, 755, 829, 1142, 1350, 1614, 1686, 3462; ¹H NMR (500 MHz, DMSO-*d*₆) δ 7.94 (dd, 1H, *J* 1.2 and 7.7 Hz), 7.88 (dd, 2H, *J* 1.2 and 8.4 Hz), 7.83-7.78 (m, 2H), 7.66 (dd, 2H, *J* 7.6 and 8.4), 7.27 (dd, 1H, *J* 1.2 and 8.2 Hz), 7.06 (s, 2H), 5.80 (s, 1H); ¹³C NMR (125 MHz APT, DMSO-*d*₆) δ 101.1, 122.8, 124.4, 126.6, 128.0, 129.3, 134.6, 134.7, 135.2, 135.2, 146.0, 150.6, 179.0, 179.7;

HRESIMS *m/z*, calcd. for C₁₆H₁₁NNaO₅S⁺ [M + Na]⁺: 352.0250, found: 352.0252.

7-Amino-5,8-dioxo-5,8-dihydronaphthalen-1-yl-4-methylbenzenesulfonate (**11b**)

Orange solid; yield > 99% (183 mg); mp 210-211 °C; IR (KBr) ν / cm⁻¹ 694, 829, 1350, 1615, 1686, 3346, 3465; ¹H NMR (500 MHz, DMSO-*d*₆) δ 2.42 (s, 3H), 5.80 (s, 1H), 7.05 (s, 2H), 7.27 (dd, 1H, *J* 0.7 and 8.2 Hz), 7.46 (d, 2H, *J* 8.5 Hz), 7.74 (d, 2H, *J* 8.4 Hz), 7.77-7.80 (m, 1H), 7.93 (dd, 1H, *J* 1.1 and 7.7 Hz); ¹³C NMR (125 MHz APT, DMSO-*d*₆) δ 20.8, 101.1, 122.9, 124.3, 126.6, 128.0, 129.7, 131.7, 135.1, 135.2, 145.6, 146.1, 150.6, 179.0, 179.4; HRESIMS *m/z*, calcd. for C₁₇H₁₃NNaO₅S⁺ [M + Na]⁺: 366.0407, found: 366.0389.

7-Amino-5,8-dioxo-5,8-dihydronaphthalen-1-yl-naphthalene-2-sulfonate (**11c**)

Orange solid; yield > 99% (203 mg); mp 230-231 °C; IR (KBr) ν / cm⁻¹ 696, 827, 1354, 1616, 1689, 3350; ¹H NMR (300 MHz, DMSO-*d*₆) δ 5.78 (s, 1H), 7.05 (s, 2H), 7.22-7.24 (m, 1H), 7.68-7.81 (m, 3H), 7.88-7.94 (m, 2H), 8.09-8.11 (m, 1H), 8.19-8.21 (m, 2H), 8.57 (d, 1H, *J* 1.3 Hz); ¹³C NMR (125 MHz APT, DMSO-*d*₆) δ 101.3, 122.3, 122.9, 124.4, 126.6, 127.7, 127.7, 129.3, 129.5, 129.6, 129.9, 131.2, 131.8, 134.9, 135.2, 135.2, 146.1, 150.6, 179.1, 179.6; HRESIMS *m/z*, calcd. for C₂₀H₁₃NNaO₅S⁺ [M + Na]⁺: 402.0407, found: 402.0405.

7-Amino-5,8-dioxo-5,8-dihydronaphthalen-1-yl-4-fluorobenzenesulfonate (**11d**)

Orange solid; yield 98% (184 mg); mp 207-208 °C; IR (KBr) ν / cm⁻¹ 696, 826, 1355, 1615, 1688, 3350; ¹H NMR (300 MHz, DMSO-*d*₆) δ 5.81 (s, 1H), 7.05 (s, 2H), 7.31 (dd, 1H, *J* 1.2 and 8.2 Hz), 7.45-7.51 (m, 2H), 7.78-7.83 (m, 1H), 7.92-7.97 (m, 3H); ¹³C NMR (125 MHz APT, DMSO-*d*₆) δ 101.9, 117.4 (d, *J* 23.0 Hz), 123.6, 125.3, 127.5, 131.6 (d, *J* 3.0 Hz), 132.1 (d, *J* 10.0 Hz), 136.0, 136.0, 146.6, 151.4, 166.1 (d, *J* 253.0 Hz), 179.8, 180.4; HRESIMS *m/z* calcd. for C₁₆H₁₀FNNaO₅S⁺ [M + H]⁺: 370.0156; found: 370.0154.

7-Amino-5,8-dioxo-5,8-dihydronaphthalen-1-yl-4-nitrobenzenesulfonate (**11e**)

Orange solid; yield 98% (198 mg); mp 213-214 °C; IR (KBr) ν / cm⁻¹ 740, 763, 832, 1348, 1618, 1682, 3364; ¹H NMR (500 MHz, DMSO-*d*₆) δ 5.81 (s, 1H), 7.06 (s, 2H), 7.31 (dd, 1H, *J* 1.2 and 8.1 Hz), 7.80-7.83 (m, 1H), 7.98 (dd, 1H, *J* 1.2 and 7.7 Hz), 8.16 (d, 2H, *J* 9.0 Hz), 8.45 (d, 2H, *J* 9.0 Hz); ¹³C NMR (125 MHz APT, DMSO-*d*₆) δ 101.2, 122.7, 124.5, 124.8, 126.8, 129.7, 135.3, 135.5, 140.0,

145.6, 150.6, 150.9, 179.1, 179.6; HRESIMS m/z , calcd. for $C_{16}H_{10}N_2NaO_7S^+ [M+Na]^+$: 397.0101, found: 397.0086.

Biological assays

Cells and virus

Vero cells (African green monkey kidney) Vero-ATCC CCL81 were cultivated in modified Dulbecco medium (DMEM, cat. No 11960, Invitrogen, São Paulo, Brazil), with routine supplementation with 5% fetal bovine serum (FBS; Invitrogen, São Paulo, Brazil), and two mmol L⁻¹ L-glutamine (cat 25030, Invitrogen, São Paulo, Brazil). Antibiotics were added, reaching a final concentration of 50 units mL⁻¹ penicillin and streptomycin (cat. No. 15070, Invitrogen, São Paulo, Brazil). The Chikungunya virus used was isolated from interviewed patients who agreed with blood collection. All patients were included by signing an informed consent form, approved by the registered research ethics committee - CAAE: 61845416.0.0000.5289. After viral isolation, the sequences were deposited in GenBank under accession numbers MK910738 (BRA/RJ/1F), MK910739 (BRA/RJ/18) and MK910740 (BRA/RJ/ 23). Virus samples were amplified in Vero cells, titrated and frozen at -70 °C for use. For antiviral activity the strain with the deposit number MK910738 was used as it is a strain with full homology to the circulating throughout Brazil.²⁷

Effect of the compounds on the cellular viability

The naphthoquinone derivatives cytotoxicity in Vero cells was evaluated using 3-(4,5-dimethylthiazol-2-yl)-2,5-diphenyltetrazolium bromide tetrazolium (MTT) reduction colorimetric assay in 96-well plate and incubated for 24 h at 37 °C.²⁸ After, naphthoquinones derivatives were added in increasing concentrations, ranging from 50 to 1000 µM, diluted in DMEM. After this period, the cells were incubated with the MTT method and evaluated in a microplate reader to determine cell viability. DMSO-treated cells (1.0%) in DMEM were used as control of the evaluation. Determination of cell viability was calculated by percentage comparing treated cells with untreated cells and cells in DMSO.

TCID₅₀ (median tissue culture infectious dose) assay for infectious virus

The effect of naphthoquinone derivatives on CHIKV replication was determined with a fixed dose of 20 µM, added to 2×10^5 infected Vero cells. This first step was to determine which key compounds were able to inhibit viral replication at this concentration and thus initiate studies with compounds that have a high inhibitory potential. Then, 2×10^5 Vero cells were plated in 24-well plate in DMEM medium with 5%

fetal bovine serum (FBS) and incubated at 37 °C at 5% CO₂. After the cells reach above 90% of confluence, the antiviral evaluation is initiated. The virus inoculum was diluted to a multiplicity of infection (MOI) of 0.1 in serum-free DMEM and added for 1 h for adsorption of viral particles at 37 °C. Afterwards, the viral inoculum was derived, the cells were washed with phosphate buffer solution (PBS) to remove non-adsorbed viral residue and fresh medium was added at the concentration of compounds. Infected cells were also treated with culture medium containing 1% DMSO to determine residual antiviral effect and ribavirin was used as a positive control for antiviral activity. After 24 h of incubation at 37 °C, the culture medium was collected and the yield of infectious virus in the cell supernatant was determined by titration using the TCID₅₀ assay on Vero cells and it was also evaluated by assay to produce viral plaques.

Virucidal profile

For the virucidal potential analysis, a mixture of 200 PFU (plaque-forming unit) containing CHIKV plus an equivalent compounds volume was prepared, varying concentrations of 5, 10, or 20 µM mL⁻¹ and incubated in microtiter plates for 2 h at 37 °C. The virus was added to Vero cells in 24-well plates for 2 h, washed, and incubated under plate assay conditions. A virucidal effect was defined as the compounds ability to inactivate the particles, blocking infection and any subsequent cytopathic effect. All treatment conditions were compared to a virus-only control.

Time-of-addition assay

To analyze the possible viral multiplication cycle stage affected by the compounds, we conducted a study with different addition times. Vero cell monolayers were grown in 24-well plates with 90% confluence. A triplicate was treated with 10 µM one hour before infection, called time -1. After one hour, the plate was fully infected with CHIKV at an MOI of 0.1, and immediately after infection, another triplicate was treated with the compounds, called time zero or concomitant. The remaining triplicates were treated according to times 1, 2, 4, 6, 8 h. After incubation for a further 12 h, the culture supernatants were collected, and the cells in the culture medium were supplemented with 3% carboxymethylcellulose. After 72 h of incubation at 37 °C, the cells were fixed with 20% formaldehyde for 2 h and stained with crystal violet for 5 min. The plaques formed after each treatment were counted, and inhibition of viral replication was determined.

Molecular docking studies

We obtained the three-dimensional structures of the potential targets of **10c** and **11a** from the Protein Data Bank

(PDB) for molecular docking purposes. The structures of CHIKV proteins were obtained under the following codes: the envelope proteins E1-E2-E3 complex (PDB 3N42),²⁹ the capsid protein (PDB 5H23)³⁰ protease domain, the protease (PDB 3TRK),³¹ and the nsP2 helicase (PDB 6JIM)³² domains, and the nsP3 (PDB 3GPO)³³ macro domain. The three-dimensional structure of **10c**, **11a**, D9, a known nsP2 protease inhibitor, and heparitin, a known envelope protein-ligand, was constructed and optimized using the Spartan'10 software (Wavefunction Inc. Irvine, CA).³⁴

Initially, the compounds were submitted to a conformational analysis using the MMFF (Merck Molecular Force Field) force field. The lowest-energy conformer was subjected to a geometry optimization using the semi-empirical RM1 method, followed by an energy calculation using the density functional theory method with B3LYP/6-311G* basis set. The molecular docking studies were performed using Autodock Tools 1.5.7 and Autodock 4.2.6.³⁵ Dockings of **10c** and **11a** into the potential targets were conducted considering the results of the experimental assays. Solvent and other artifact molecules were removed from the protein structures. Autodock Tools was used to add polar hydrogens and Gasteiger charges. Proteins were considered rigid, while total flexibility of ligands was allowed. The grid box for each protein was defined according to their binding sites described in the literature: the heparan-sulfate-binding and the predicted binding pocket 1 sites of the envelope protein, the active (comprising the catalytic triad) and the hydrophobic (where E2 protein interacts with the capsid protein) sites, the active site of nsP2 protease, the adenosine triphosphate (ATP) binding site of nsP2 helicase, and the ADP-ribose binding site of nsP3.³⁶⁻³⁸

The Lamarckian genetic algorithm was employed, and a total of 50 binding poses were calculated for each binding site. The pose with the lowest binding energy was selected for evaluation. The potential target of **10c** and **11a** was elected based on the binding energy and visual inspection of the binding mode and interaction analysis compared with known ligands. These analyses were realized using the Discovery Studio Visualizer 2019 (Dassault Systèmes BIOVIA, San Diego, 2019)³⁹ and Pymol version 2.5 (The PyMOL Molecular Graphics System, version 2.5, Schrödinger, LLC).⁴⁰

Statistical analysis

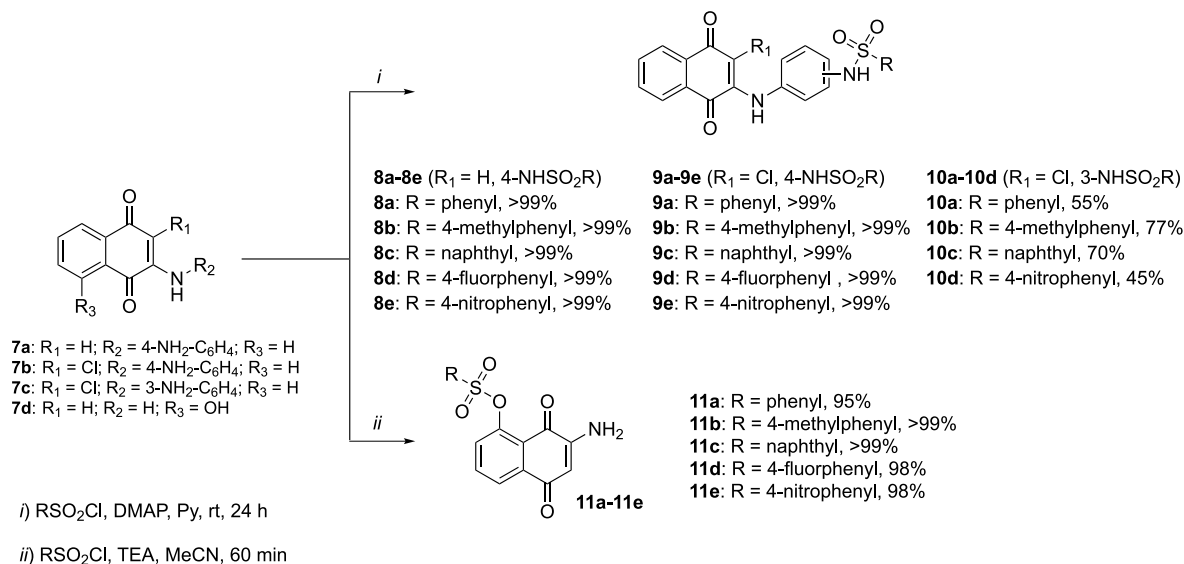
The data were analyzed by one-way analysis of variance (ANOVA) followed by Tukey's post-test using the GraphPad Instat version 3 program.⁴¹ A *p*-value of < 0.05 was considered statistically significant.

Results and Discussion

Chemistry

The amino-naphthoquinones (**7a-7d**) used as starting material for the preparation of sulfonamide-based naphthoquinones derivatives were prepared according to the reported methodology.^{42,43} Subsequently, the desired sulfonamide derivatives (**8a-8e**, **9a-9e**, and **10a-10d**) were obtained in one step by choosing the appropriate amino-naphthoquinones (**7a-7c**) with various aryl sulfonyl chlorides catalyzed by DMAP in pyridine. The overall yield calculated after column chromatography purification ranged from 45-99%. Spectroscopic techniques confirmed the structures of all final compounds (**8-10**). In general, the FTIR analysis of sulfonamide derivatives exhibited absorption bands at 1600-1680 cm⁻¹, referring to the stretch vibrations of C=O bonds. It was possible to observe absorption bands of medium intensity in the region between 3100-3300 cm⁻¹, corresponding to the stretch vibrations of N-H bonds. The analysis also showed absorptions at 1150-1330 cm⁻¹, referring to asymmetric and symmetrical stretching of the SO₂ group bounds. In the ¹H NMR of the compound **8b**, two singlets, 8.91 and 10.09 ppm were assigned to the N-H bonds hydrogens of the sulfonamide and amino group. Regarding the naphthoquinone nucleus, it could be observed a singlet at 5.96 ppm corresponding to H-3 hydrogens and two double doublets at 8.03 ppm (dd, 1H, *J* 7.6 and 1.0 Hz, 1H) and 7.94 ppm (dd, 1H, *J* 7.6 and 1.0 Hz, 1H), corresponding to typical benzoaromatic hydrogens. The other signals referring to the remaining aromatic hydrogens were observed. The other signals referring to aromatic hydrogens were observed as characteristic double signals at 7.15 ppm (d, 2H, *J* 8.9 Hz, 2H), 7.24 ppm (d, 2H, *J* 8.9 Hz, 2H), 7.34 ppm (d, 2H, *J* 8.3 Hz, 2H) and 7.66 ppm (d, 2H, *J* 8.3 Hz, 2H).

The sulfonated naphthoquinones derivatives (**11a-11e**) were also prepared in a single step by treating a solution of **7d** in acetonitrile with triethylamine (TEA) and the appropriate sulfonyl chlorides. The products were obtained with excellent yields ranging from 95-99% (Scheme 1). Spectroscopic techniques also confirmed the chemical structures of these compounds. For example, in the ¹H NMR of the compound **11b**, it was possible to show that the sulfonylation reaction proceeded in the hydroxyl group by the absence of a characteristic signal referring to hydroxyl hydrogens. Another evidence is a singlet at 7.05 ppm (s, 2H) corresponding to amino hydrogens. Besides, it is possible to observe the presence of two sets of signals referring to the aromatic hydrogens of the sulfonic ester group: two doublet signals at 7.74 ppm (d, 2H, *J* 8.4 Hz, 2H) and



Scheme 1. Synthetic strategy to obtain naphthoquinones derivatives **8-11**.

7.46 ppm (d, 2H, *J* 8.5 Hz, 2H); and a singlet at 2.42 ppm (s, 3H), corresponding to a methyl group.

Biological assays

Cytotoxicity of naphthoquinone derivatives and antiviral effect

The MTT assay was used to determine the cytotoxicity of each naphthoquinone derivatives to Vero cells. The 50% cytotoxic concentration (CC₅₀) value of each compound was calculated (Table 1). According to our results, no high cytotoxicity was observed for all tested compounds and no cytotoxicity in cells treated with 0.1% DMSO (final solvent concentration used to dissolve naphthoquinone in the cell culture medium). After determining cytotoxicity, the compounds were used in a fixed dose (20 μM) to determine whether they would be able to inhibit CHIKV replication in Vero cells. In the initial evaluation, the compounds **9b**, **9e**, **10c**, **11a**, and **11b** showed an inhibition effect above 98% of CHIKV replication at this fixed concentration (Table 1).

Determination of the effect of naphthoquinone derivatives on CHIKV replication

The antiviral effect evaluation was performed in Vero cells for all substances that affected greater than 90%. Vero cells were infected with CHIKV using a multiplicity of infection (MOI) of 0.1 and treated for 24 h with increasing substances concentrations. The TCID₅₀ method was used to titrate the virus yield, and the concentration capable of reducing the virus yield by 50% (EC₅₀) was obtained from a dose-response curve, and the values are shown in Table 2 and Figure 2. The relationship between cytotoxicity

Table 1. Cytotoxicity (CC₅₀) and anti-CHIKV activities at 20 μM of naphthoquinone derivatives

Compound	CC ₅₀ / μM	Inhibition of viral replication / %
8a	354 ± 3.8	60 ± 3.9
8b	201 ± 4.6	59 ± 3.6
8d	307 ± 5.5	40 ± 3.3
8c	449 ± 4.7	49 ± 4.0
8e	287 ± 5.2	45 ± 3.0
9a	300 ± 4.4	52 ± 2.0
9b	281 ± 2.5	99 ± 4.3
9d	331 ± 3.3	80 ± 4.2
9c	435 ± 3.9	34 ± 3.3
9e	540 ± 3.7	98 ± 3.5
10a	399 ± 5.5	35 ± 1.35
10b	446 ± 4.8	23 ± 1.5
10c	322 ± 6.5	99 ± 2.9
10d	529 ± 3.5	42 ± 3.4
11a	352 ± 4.3	99 ± 4.1
11b	478 ± 6.2	99 ± 3.9
11c	196 ± 4.8	12 ± 0.8
11d	329 ± 5.6	20 ± 1.6
11e	233 ± 6.8	35 ± 2.4

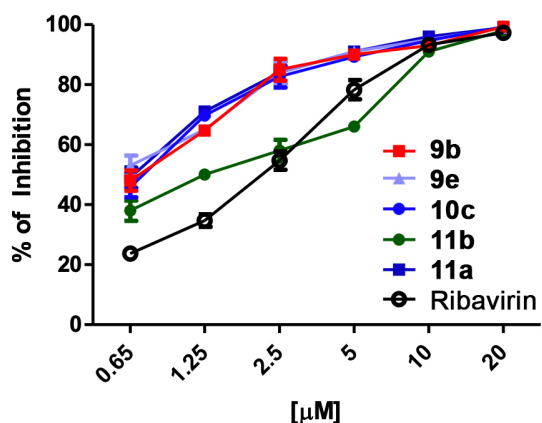
The mean values ± standard deviations are representative of three independent experiments.

and the compound antiviral effect was assessed using the selectivity index (SI ratio, CC₅₀/EC₅₀) and determined for each molecule, obtaining unit values. As observed in Table 2, five naphthoquinone derivatives, **9b**, **9e**, **10c**, **11a**, and **11b**, showed an expressive SI for CHIKV, with 289, 457, 418, 400, and 382, respectively. In the same way, in Figure 2, we can observe a dose-dependent response on the inhibitory effects obtained by the substances assessed. Ribavirin was used as a control (Table 2).

Table 2. Cytotoxicity (CC_{50}), anti-CHIKV profile (EC_{50}) and selectivity index (SI) of naphthoquinones

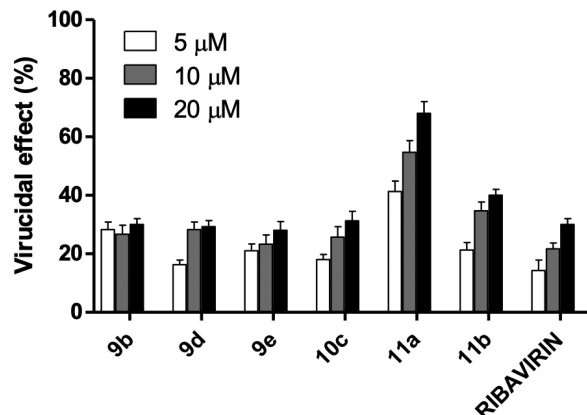
Compound	CHIKV		
	$CC_{50}^a / \mu\text{M}$	$EC_{50}^b / \mu\text{M}$	SI ^c
8c	449 ± 4.7	ND	–
9b	281 ± 2.5	0.97 ± 0.2	289
9d	331 ± 3.3	3.27 ± 0.6	101
9e	540 ± 3.7	1.18 ± 0.16	457
10c	322 ± 6.6	0.77 ± 0.1	418
10d	529 ± 3.5	ND	–
11a	352 ± 4.3	0.88 ± 0.1	400
11b	478 ± 6.2	1.25 ± 0.2	382
11e	233 ± 6.8	ND	–
Ribavirin	297 ± 4.2	2.42 ± 0.5	122

^aConcentration that reduced 50% cytotoxic concentration when compared to untreated controls; ^bconcentration that reduced 50% of CHIKV replication when compared to infected controls; ^cselectivity index was defined as the ratio between CC_{50} and EC_{50} and represents the safety for *in vitro* assays. The mean values ± standard deviations are representative of three independent experiments. CHIKV: Chikungunya virus; ND: not detected.

**Figure 2.** Inhibition of CHIKV replication by naphthoquinone derivatives and ribavirin. Vero cells were infected with CHIKV and treated at concentrations of 0.65, 1.25, 2.5, 5, 10, and 20 μM . Data are presented as percentage of virus titer when compared to control cells and are expressed as the mean of three experiments ± standard error.

Virucidal effect

Given all the tested compounds, at least five derivatives exhibited a significant inhibitory profile for CHIKV replication with low cytotoxicity. A crucial step in discovering the mechanism of action is evaluating the compound's effect on the viral particle. For this reason, we determined the virucidal potential of the compounds. Our results showed that of the five compounds tested, only **11a** presented some virucidal effect in the tested concentrations. As shown in Figure 3, the compound **11a** was able to inhibit above 70% in the treatment with 20 μM . Interestingly, ribavirin at the same concentrations did not exhibit virucidal potential.

**Figure 3.** Naphthoquinone derivatives effect on the CHIKV infectivity. Vero cells were infected with CHIKV at an MOI of 0.1, and a plaque assay evaluated the results. Error bars indicate the standard deviation. Experiments were performed in triplicate.

Time-of-addition studies

A time-of-addition experiment was conducted to identify at which point of the CHIKV replication cycle the substances exert their specific antiviral effect. All compounds already have an antiviral effect at time 0 (concomitant) to infection, inhibiting above 90% of viral replication at the concentration used (10 μM).

The substance **11a** showed a differentiated profile, since, at point -1, it presented an inhibitory potential of approximately 70%, increasing its effect for up to 2 h post-infection, reaching inhibition above 90% at time 0, maintaining inhibition above 80% until the second hour, declining sharply after 4 h post-treatment, falling below 40% inhibition. The other substances showed a greater inhibitory potential in the treatment times of 0, 1, and 2 h, decreasing progressively after the other times, reaching an inhibitory potential below 40%. Conversely, compound **10c** showed low inhibitory potential at time -1, although 0 inhibiting replication above 90%, maintaining potent inhibition until 8 h post-infection (Figure 4). Time dependence on the inhibitory effect of compound **11a** is consistent with the hypothesis that its anti-CHIKV appears to be in events before entry. The compound **10c** showed an inhibitory effect with more consistent post-infection effects.

In silico prediction of the antiviral targets

In silico target prediction of **10c**

According to the antiviral assays, we observed that **10c** had no significant effect on the CHIKV particle infectivity but inhibited virus replication when added during attachment and later, which, in turn, indicates that this compound acts on post-entry steps. To evaluate the potential targets of this compound, we docked **10c** with the available crystallographic structures of CHIKV proteins

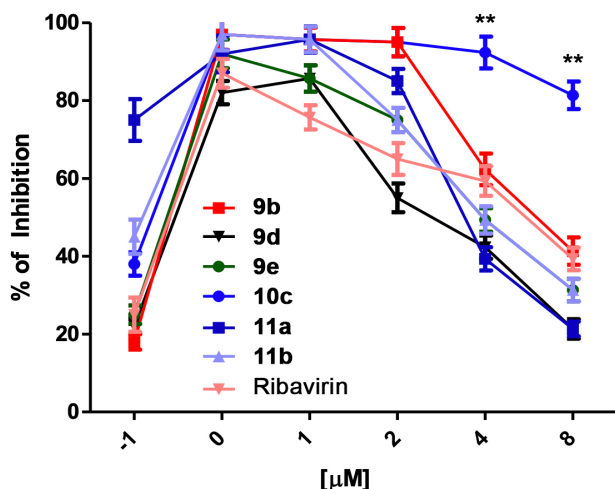


Figure 4. Effect of the addition of the naphthoquinone derivatives on replication over time. Monolayers of Vero cells were infected with CHIKV at an MOI of 0.1 at time -1 , zero, and up to 8 h. At times indicated, compounds or ribavirin was added to a final concentration of $10 \mu\text{g mL}^{-1}$. Data are presented as percentage of virus titer, when compared to control cells and are expressed as the mean of three experiments \pm standard error. Statistical analysis was performed using the Tukey's test to compare naphthoquinone derivatives with ribavirin in each time: $**p < 0.01$.

essential in post-entry stages, like capsid protein (protease domain), nsP2 (helicase and protease domains), and nsP3 (macro domain).

Among the proteins evaluated, **10c** exhibited the highest theoretical binding affinity with nsP3 ($-9.02 \text{ kcal mol}^{-1}$). **10c** showed a slightly bent conformation bound to nsP3, which is very similar to the co-crystallized ligand ADP-ribose (Figure 5). The naphthoquinone ring of **10c** occupied the same region of the phosphates and distal ribose groups and was hydrogen-bonded to V33, C34, and Y114. Also, we observed that this ring was involved in a T-shaped π - π stacking interaction with Y114 and van der Waals contacts with N24 and V113. The sulfonamide and the central phenyl groups of **10c** were positioned at the binding region of the co-crystallized ligand adenosine ribose. They established a double hydrogen-bond with L108 and a van der Waals contact with G112. The naphthalene moiety bound in the same region as observed for the adenine group of ADP-ribose and established van der Waals interactions with I11, C143, and R144.

Furthermore, the extended effect observed in the time-of-addition assay suggested that this compound may have a multi-target mechanism of action. **10c** showed the second strongest binding affinity with nsP2 protease ($-7.08 \text{ kcal mol}^{-1}$). Also, we docked the known inhibitor D9 18 with this protease for comparison purposes. **10c** presented an extended binding mode as observed for the inhibitor (Figure 5). The naphthoquinone ring was positioned in the S2 subsite. This molecule was anchored by several interactions, such as a hydrogen bond with W1084,

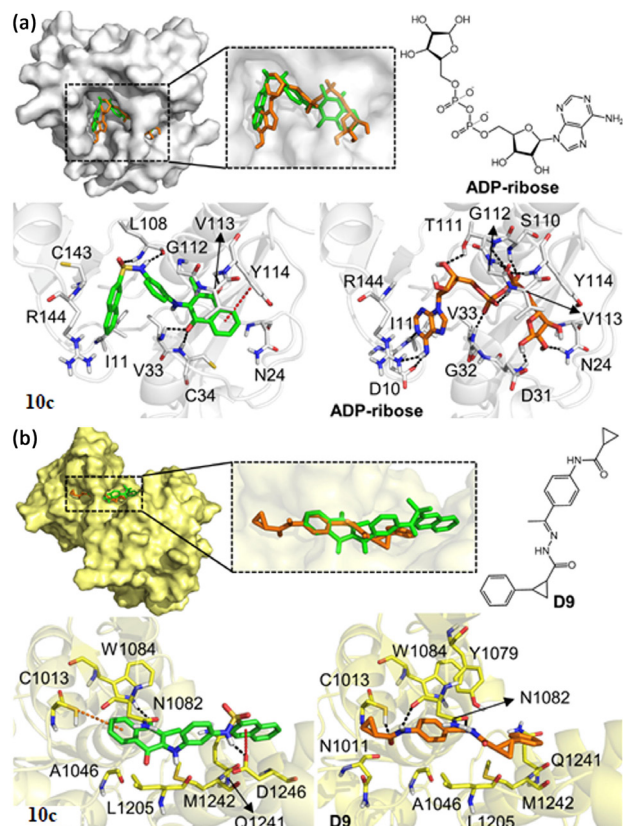


Figure 5. Docking of **10c** with its potential anti-CHIKV targets. Binding mode and molecular interactions of (a) **10c** (green) and the co-crystallized inhibitor adenosine diphosphate ribose (ADP-ribose, orange) with the macro domain of nsP3, and (b) **10c** (green) and the known inhibitor D9 (orange) with the nsP2 protease. Hydrogen bonds are described as black dashed lines, anion- π or π - π stacking interactions are shown as red dashed lines, and π -sulfur interaction is represented as orange dashed line.

a π -sulfur interaction with the catalytic C1013 residue, and van der Waals contacts with A1046, N1082, and L1205. The central phenyl group of **10c** bound at the S3 subsite of the protease and interacted with M1242. Like the distal phenyl and cyclopropyl rings of D9, the sulfonamide and naphthalene groups of **10c** explored the S4 subsite. The sulfonamide group was hydrogen-bonded with D1246. This residue was also anchoring the naphthalene ring by an anion- π interaction in addition to the van der Waals contact with Q1241.

Moreover, **10c** was docked to the capsid protein and nsP2 helicase. However, it had the lowest theoretical affinity (-6.25 and $-5.50 \text{ kcal mol}^{-1}$ for the active and capsid protein hydrophobic sites, respectively, and $-5.06 \text{ kcal mol}^{-1}$ nsP2 helicase). This prototype did not exhibit a binding manner similar to known ligands of these proteins (data not shown).

In silico target prediction of **11a**

Unlike **10c**, **11a** showed a direct effect on virus particles and acted in the early stages of the CHIKV lifecycle. So, we investigated *in silico* whether this compound could bind

to the envelope proteins and the nsP2 protease and helicase domains and nsP3 macro domain.

11a showed the highest theoretical affinity with the macro domain of nsP3 (-5.10 kcal mol $^{-1}$). The naphthoquinone moiety was aligned with the adenosine ribose group of ADP-ribose and was involved in a hydrogen bond interaction with L108 and van der Waals contacts with A22, V33, T111, and W148 (Figure 6a). On the other hand, the sulfone and phenyl groups were positioned at the same binding region as observed for the known ligand phosphates and distal ribose. Consequently, **11a** was allowed to establish similar interactions with the protein. The sulfone group interacted with V33 and V113 by hydrogen bonding. Besides, the phenyl ring was π -stacked with Y114 and interacted with V113 via van der Waals contact.

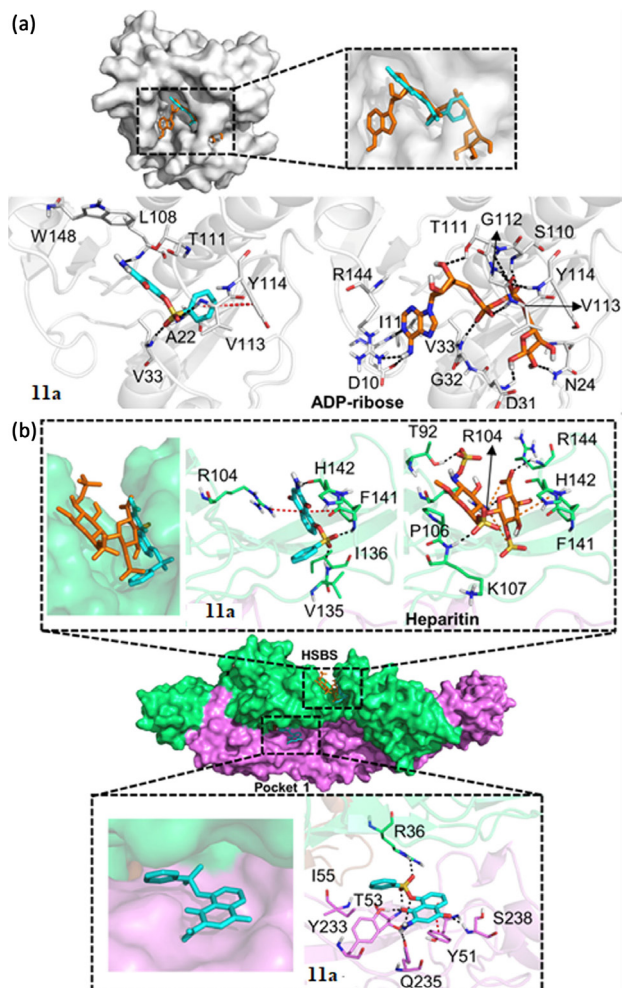


Figure 6. Docking of **11a** with its potential anti-CHIKV targets. Binding mode and molecular interactions of (a) **11a** (cyan) and the co-crystallized inhibitor ADP-ribose (orange) with the macro domain of nsP3, and (b) **11a** (cyan) and the heparan sulfate disaccharide, heparin (orange), within the heparan-sulfate binding site (HSBS) and pocket 1 of the CHIKV envelope protein complex. E1, E2, and E3 are colored in violet, green and brown, respectively. Hydrogen bonds are exhibited as black dashed lines, cation- π or π - π stacking interactions are shown as red dashed lines, and ionic interactions are represented as orange dashed lines.

Following nsP3, **11a** showed the second strongest theoretical affinity with the CHIKV envelope proteins. Two binding sites were explored, and **11a** presented a similar affinity towards pocket 1 (-4.57 kcal mol $^{-1}$) compared to the heparan-sulfate-binding site (-4.46 kcal mol $^{-1}$). At pocket 1, the naphthoquinone nucleus was π -stacked with Y51 and hydrogen-bonded to Y233 and S238 of E1 (Figure 6b). Also, the sulfone group established hydrogen bond interactions with the side chain of R36 of E2 and with the principal and side chains of T53 of E1, while the phenyl ring was involved in van der Waals contacts with I55 from E1. For the heparan-sulfate binding site, the naphthoquinone ring was sandwiched between R104 and F141 by cation- π and π - π stacking interactions, respectively, while the amino group was hydrogen-bonded to H142 (Figure 6b). The sulfone group established hydrogen bond interactions with V135 and F141, whereas the phenyl ring was involved in a van der Waals interaction with I136. Interestingly, we observed that **11a** explored the same binding region as one of the sulfated saccharide nuclei of heparin (a heparan sulfate disaccharide used as a control herein) and shared interactions R104, F141, and H142. Additionally, **11a** showed the lowest theoretical binding affinity with both protease and helicase domains of CHIKV nsP2 (-4.35 and -3.61 kcal mol $^{-1}$, respectively) (data not shown).

The cell viability assay revealed a low toxic potential for all compounds. Remarkably, compounds **9b**, **9e**, **10c**, **11a**, and **11b** exhibited potent inhibitory activity with a highly selective index. We highlight compounds **9e** and **10c** that presented EC $_{50}$ equal to 1.18 and 0.77 μ M, generating SI of 457 and 418, respectively. In contrast, ribavirin, which is an escort drug for clinical use and used as a control, shows a lower inhibitory potential with 2.42 μ M of EC $_{50}$ and SI of 122.

Compound **11a** showed a virucidal effect above 40% at 5 μ M, reaching above 70% at 20 μ M, demonstrating that possibly most of its antiviral effects are at the earliest moments of the viral infection process. These results are in accordance with the time-of-addition assays showed that all compounds already had an antiviral effect at time 0 to infection. The addition time tests showed that although all compounds already had an antiviral effect at time 0 of infection, compound **11a** already has an early inhibitory potential (-1) that is, still in pre-treatment, maintaining its inhibitory potential until 2 h post-infection, with its inhibitory potential declining rapidly, reaching an inhibitory effect of less than 40% at 4 h post-infection (Figure 4).

We highlight compounds **9e** (CC $_{50}$ = 540) and **10c** (CC $_{50}$ = 322) and they presented EC $_{50}$ equal to 1.18 and 0.77 μ M, generating SI of 457 and 418, respectively. These results prove to be promising, requiring further studies that

can describe in greater depth the mechanism of action of these compounds. Taking into account that there are no specific medicines for the treatment of infections caused by arboviruses, it is important to search for substances that can be used in the control, treatment and prevention of these infections in order to reduce morbidity and mortality rates caused by CHIKV.

In contrast, compound **11a** presented a differentiated profile consistent with action on events before entry. Only the compound **10c** showed an inhibitory effect consistent with post-infection effects. *In silico* studies, some molecular targets may explain these differences in these compound mechanisms of action. Therefore, our results indicate that these compounds can serve as promising scaffolds for developing specific inhibitors for the proliferation of CHIKV.

According to the experimental assay, we conducted computational studies to get more insights into the antiviral targets of the most potent compounds **10c** and **11a**. Both compounds showed the strongest binding affinity with the macro domain of nsP3. Many contacts observed for both compounds (e.g., V33, T111, V113, and Y114) were proved to be essential for ligand binding into the macro domain of CHIKV nsP3 by structural and computational methods, which reinforces the potential of these naphthoquinone derivatives to inhibit this enzyme. Interestingly, the druggability of CHIKV nsP3 has been recently demonstrated.^{44,45} The precise role of this protein in CHIKV replication remains to be fully understood, but it is essential for several steps in virus replication like genome replication, viral assembly, and host cell shutdown.^{46,47} This protein is also involved in the virulence and pathogenesis of the alphaviruses.^{48,49}

Although these derivatives likely share a similar target at early steps of virus replication, the mechanistic studies indicated that these compounds might act at different targets as well. The activity of **10c** was prolonged and observed only at post-entry steps. Our *in silico* strategy also suggested that it could also inhibit the CHIKV nsP2 protease. This protein is responsible for the polyprotein processing of CHIKV, which is crucial for virus replication.^{50,51} Despite the lack of experimental data regarding the structural basis for CHIKV nsP2 protease inhibition, mutation and computational studies have provided valuable information to date. For instance, C1013, N1082, H1083, and W1084 are required for the maintenance of the protease activity of alphavirus nsP2.^{52,53} In this context, the hydrogen bond with W1084 seems to be a critical interaction for its inhibition.^{54,55} As well, interactions with residues C1013, A1046, N1082, W1084, and L1205 are commonly observed in the design of novel inhibitors.⁵⁶ It is important to note that **10c** interacted with all these residues like the known inhibitor D9.

Additionally, inhibitors of CHIKV nsP2 protease

have shown their antiviral activity at the early stages of viral replication, which agrees with the experimental data obtained in this work.^{57,58}

On the other hand, **11a** was also shown to act directly on virus particles. Interestingly, this compound showed the second-highest theoretical binding affinity with two sites of the CHIKV envelope protein. Pocket 1 was predicted by computational tools and is found between the domain II of E1 and β -ribbon of E2. Targeting this site could stabilize the envelope complex, prevent E1-E2 dissociation, and, consequently, block fusion process.⁵⁹ Indeed, **11a** presented similar interactions as potential ligands of this site.^{35,54} Additionally, **11a** bound to the heparan-sulfate binding site with a similar affinity as heparitin. It could establish important interactions like the one with the key residue R104, which, in turn, could impair the virus-cell interaction and inhibit the virus entry. In either case, the binding towards envelope proteins may contribute to inhibition of the viral particle production observed when the compound is added during or a little after virus attachment.³⁴ Our results showed the promising potential of **10c** and **11a**, and further experimental assays with the putative targets should be performed to confirm our predictions.

Conclusions

In this work, we report the synthesis of nineteen compounds containing a sulfonamide or sulfonate group attached to a naphthoquinone framework. The compounds were assessed *in vitro* for their anti-viral activity towards CHIKV. The cell viability assay revealed low toxic potential for all compounds. Remarkably, compounds **9b**, **9e**, **10c**, **11a** and **11b** exhibited potent inhibitory activity with high selective index. Among them, the compound **11a** also showed strong virucide effect. Time-of-addition assays showed that all compounds already had an antiviral effect at time 0 to infection, whereas the compound **11a** presented a differentiated profile consistent with post entry inhibitory action with a virucidal effect above 40% at 5 μ M, reaching above 70% at 20 μ M, demonstrating that possibly most of its antiviral effects are at the earliest moments of the viral infection process. Collectively, our findings also suggested that **10c** and **11a** share the macro domain of nsP3 as a common antiviral target. In addition, **10c** likely inhibits the nsP2 protease, while **11a** seems to bind to the envelope protein to inhibit virus entry and fusion processes as well.

Supplementary Information

Supplementary data are available free of charge at <http://jbcbs.sbj.org.br> as PDF file.

Acknowledgments

This work was partially supported by FAPERJ grant numbers E-26/203.191/2017, E-26/010.101106/2018, E-26/202.800/2017, E-26/010.003002/2014, E-26/203.246/2017, and E-26/202.353/2019; CNPq 301873/2019-4, 306011/2020-4, 308755/2018-9, and CAPES Financial Code 001.

Author Contributions

Paulo A. F. Pacheco was responsible for organic synthesis work; Daniel T. Gonzaga for organic synthesis work; Cláudio C. Cirne-Santos for biological assays work; Caroline S. Barros for biological assays work; Max W. L. Gomes for biological assays work; Rafaela S. P. Gomes for biological assays work; Mariana C. Gonçalves for biological assays work; Vitor F. Ferreira for coordination of organic synthesis work, contributions to manuscript writing; Vitor W. Rabelo for biological assays work; Paula A. Abreu for biological assays work; Robson X. Faria for coordination of biological assays, contributions to manuscript writing; Gabriel O. de Resende for coordination of organic synthesis work, contributions to manuscript writing; David R. da Rocha for coordination of organic synthesis work, contributions to manuscript writing; Izabel C. N. de P. Paixão for biological assays work; Fernando C. da Silva for coordination of organic synthesis work, contributions to manuscript writing.

References

- Thomson, R. H.; *Naturally Occurring Quinones IV*; Springer: Netherlands, 1996.
- Monks, T.; Jones, D.; *Curr. Drug Metab.* **2005**, *3*, 425.
- Dias, F. R. F.; Guerra, F. S.; Lima, F. A.; de Castro, Y. K. C.; Ferreira, V. F.; Campos, V. R.; Fernandes, P. D.; Cunha, A. C.; *J. Braz. Chem. Soc.* **2021**, *32*, 476.
- Novais, J. S.; Rosandiski, A. C.; de Carvalho, C. M.; Silva, L. S. S.; de Souza, L. C. S. V.; Santana, M. V.; Martins, N. R. C.; Castro, H. C.; Ferreira, V. F.; Gonzaga, D. T. G.; de Resende, G. O.; da Silva, F. C.; *Curr. Top. Med. Chem.* **2019**, *20*, 121.
- Luo, P.; Wong, Y. F.; Ge, L.; Zhang, Z. F.; Liu, Y.; Liu, L.; Zhou, H.; *J. Pharmacol. Exp. Ther.* **2010**, *335*, 735.
- Wang, R.; Hu, Q.; Wang, H.; Zhu, G.; Wang, M.; Zhang, Q.; Zhao, Y.; Li, C.; Zhang, Y.; Ge, G.; Chen, H.; Chen, L.; *Int. J. Biol. Macromol.* **2021**, *183*, 182.
- BACTRIM™*; https://www.accessdata.fda.gov/drugsatfda_docs/label/2003/17377slr057_Bactrim_lbl.pdf, accessed in January 2022.
- Qiu, H. Y.; Wang, P. F.; Lin, H. Y.; Tang, C. Y.; Zhu, H. L.; Yang, Y. H.; *Chem. Biol. Drug Des.* **2018**, *91*, 681.
- Hook, I.; Mills, C.; Sheridan, H. In *Studies in Natural Products Chemistry*; Atta-ur-Rahman, ed.; Elsevier: Oxford, 2014, ch. 5.
- Rougeron, V.; Sam, I. C.; Caron, M.; Nkoghe, D.; Leroy, E.; Roques, P.; *J. Clin. Virol.* **2015**, *64*, 144.
- Plotkin, S. A.; *J. Pediatr. Infect. Dis. Soc.* **2019**, *8*, 95.
- Kucharz, E. J.; Cebula-Byrska, I.; *Eur. J. Intern. Med.* **2012**, *23*, 325.
- Weaver, S. C.; Lecuit, M.; *N. Engl. J. Med.* **2015**, *372*, 1231.
- Sharif, N.; Sarkar, M. K.; Ferdous, R. N.; Ahmed, S. N.; Billah, M. B.; Talukder, A. A.; Zhang, M.; Dey, S. K.; *Front. Microbiol.* **2021**, *12*, 689979.
- Silva, J. V. J.; Ludwig-Begall, L. F.; de Oliveira-Filho, E. F.; Oliveira, R. A. S.; Durães-Carvalho, R.; Lopes, T. R. R.; Silva, D. E. A.; Gil, L. H. V. G.; *Acta Trop.* **2018**, *188*, 213.
- McArthur, D. B.; *Nurs. Clin. North Am.* **2019**, *54*, 297.
- Hucke, F. I. L.; Bugert, J. J.; *Front. Public Health* **2020**, *8*, 618624.
- Acetazolamide*; <https://www.drugs.com/monograph/acetazolamide.html>, accessed in January 2022.
- CDER Statement: FDA Approves Labeling Supplement for Celebrex (celecoxib)*; <https://www.fda.gov/drugs/drug-safety-and-availability/cder-statement-fda-approves-labeling-supplement-celebrex-celecoxib>, accessed in January 2022.
- DiaBeta® (glyburide) Tablets USP*; https://www.accessdata.fda.gov/drugsatfda_docs/label/2009/017532s030lbl.pdf, accessed in January 2022.
- Murthy, I. S.; Sireesha, R.; Deepti, K.; Srinivasa Rao, P.; Ramesh Raju, R.; *Chem. Data Collect.* **2021**, *31*, 100608.
- Uma Priya, K.; Venkataramaiah, C.; Sreedhar, N. Y.; Raju, C. N.; *RSC Adv.* **2021**, *11*, 3897.
- Manolov, S. P.; Ivanov, I. I.; Bojilov, D. G.; *J. Serb. Chem. Soc.* **2021**, *86*, 139.
- Gulçin, İ.; Taslimi, P.; *Expert Opin. Ther. Pat.* **2018**, *28*, 541.
- AGENERASE™*; https://www.accessdata.fda.gov/drugsatfda_docs/label/1999/21007lbl.pdf, accessed in January 2022.
- PREZISTA (darunavir)*; https://www.accessdata.fda.gov/drugsatfda_docs/label/2012/021976s0211lbl.pdf, accessed in January 2022.
- Cirne-Santos, C. C.; Barros, C. S.; Nogueira, C. C. R.; Azevedo, R. C.; Yamamoto, K. A.; Meira, G. L. S.; de Vasconcelos, Z. F. M.; Ratcliffe, N. A.; Teixeira, V. L.; Schmidt-Chanasit, J.; Ferreira, D. F.; Paixão, I. C. N. P.; *Front. Microbiol.* **2019**, *10*, 2426.
- Mosmann, T.; *J. Immunol. Methods* **1983**, *65*, 55.
- 3N42. Crystal Structures of the Mature Envelope Glycoprotein Complex (furin cleavage) of Chikungunya virus*; <https://www.rcsb.org/structure/3N42>, accessed in January 2022.
- 5H23. Crystal Structure of Chikungunya Virus Capsid Protein*; <https://www.rcsb.org/structure/5H23>, accessed in January 2022.
- 3TRK. Structure of the Chikungunya Virus nsP2 Protease*; <https://www.rcsb.org/structure/3TRK>, accessed in January 2022.

32. 6JIM. *Viral Helicase Protein*; <https://www.rcsb.org/structure/6JIM>, accessed in January 2022.
33. 3GPO. *Crystal Structure of Macro Domain of Chikungunya Virus in Complex with ADP-ribose*; <https://www.rcsb.org/structure/3GPO>, accessed in January 2022.
34. *Spartan*, version 10; Wavefunction, Inc., Japan Branch Office, Japan, 2011.
35. Molecular Graphics Laboratory; *Autodock Tools*, version 1.5.7; The Scripps Research Institute, USA, 2010.
36. Sahoo, B.; Chowdary, T. K.; *Biosci. Rep.* **2019**, *39*, BSR20191077.
37. Nguyen, P. T. V.; Yu, H.; Keller, P. A.; *Interdiscip. Sci.: Comput. Life Sci.* **2018**, *10*, 515.
38. Sharma, R.; Kesari, P.; Kumar, P.; Tomar, S.; *Virology* **2018**, *515*, 223.
39. *Discovery Studio Visualizer* 2019, Dassault Systèmes BIOVIA, San Diego, 2019.
40. The PyMOL Molecular Graphics System, *Pymol*, version 2.5; Schrödinger, LLC, 2018.
41. *GraphPad InStat*, version 3; GraphPad Software, Inc.; USA, 2001.
42. Couladouros, E. A.; Plyta, Z. F.; Haroutounian, S. A.; Papageorgiou, V. P.; *J. Org. Chem.* **1997**, *62*, 6.
43. Giordano, A.; Powers, G. D.; Sturgess, M. A.; Yang, K.; *US-6630589-B1*, **2007**.
44. Malet, H.; Coutard, B.; Jamal, S.; Dutartre, H.; Papageorgiou, N.; Neuvonen, M.; Ahola, T.; Forrester, N.; Gould, E. A.; Lafitte, D.; Ferron, F.; Lescar, J.; Gorbalenya, A. E.; de Lamballerie, X.; Canard, B.; *J. Virol.* **2009**, *83*, 6534.
45. Puranik, N. V.; Rani, R.; Singh, V. A.; Tomar, S.; Puntambekar, H. M.; Srivastava, P.; *ACS Omega* **2019**, *4*, 20335.
46. Abraham, R.; Hauer, D.; McPherson, R. L.; Utt, A.; Kirby, I. T.; Cohen, M. S.; Merits, A.; Leung, A. K. L.; Griffin, D. E.; *Proc. Natl. Acad. Sci. U. S. A.* **2018**, *115*, E10457.
47. Gao, Y.; Goonawardane, N.; Ward, J.; Tuplin, A.; Harris, M.; *PLoS Pathog.* **2019**, *15*, e1007239.
48. Abraham, R.; McPherson, R. L.; Dasovich, M.; Badiee, M.; Leung, A. K. L.; Griffin, D. E.; *mBio* **2020**, *11*, e03253.
49. Meertens, L.; Hafirassou, M. L.; Couderc, T.; Bonnet-Madin, L.; Kril, V.; Kümmerer, B. M.; Labeau, A.; Brugier, A.; Simon-Loriere, E.; Burlaud-Gaillard, J.; Doyen, C.; Pezzi, L.; Goupil, T.; Rafasse, S.; Vidalain, P. O.; Bertrand-Legout, A.; Gueneau, L.; Juntas-Morales, R.; Ben Yaou, R.; Bonne, G.; de Lamballerie, X.; Benkirane, M.; Roingeard, P.; Delaugerre, C.; Lecuit, M.; Amara, A.; *Nature* **2019**, *574*, 259.
50. Rupp, J. C.; Sokoloski, K. J.; Gebhart, N. N.; Hardy, R. W.; *J. Gen. Virol.* **2015**, *96*, 2483.
51. Shin, G.; Yost, S. A.; Miller, M. T.; Elrod, E. J.; Grakoui, A.; Marcotrigiano, J.; *Proc. Natl. Acad. Sci. U. S. A.* **2012**, *109*, 16534.
52. Narwal, M.; Singh, H.; Pratap, S.; Malik, A.; Kuhn, R. J.; Kumar, P.; Tomar, S.; *Int. J. Biol. Macromol.* **2018**, *116*, 451.
53. Strauss, E. G.; de Groot, R. J.; Levinson, R.; Strauss, J. H.; *Virology* **1992**, *191*, 932.
54. Giacotti, G.; Cancellieri, M.; Balboni, A.; Giustiniano, M.; Novellino, E.; Delang, L.; Neyts, J.; Leyssen, P.; Brancale, A.; Bassetto, M.; *Eur. J. Med. Chem.* **2018**, *149*, 56.
55. Tardugno, R.; Giacotti, G.; de Burghgraeve, T.; Delang, L.; Neyts, J.; Leyssen, P.; Brancale, A.; Bassetto, M.; *Bioorg. Med. Chem.* **2018**, *26*, 869.
56. Rabelo, V. W. H.; Paixão, I. C. N. P.; Abreu, P. A.; *Expert Opin. Ther. Targets* **2020**, *24*, 63.
57. Das, P. K.; Puusepp, L.; Varghese, F. S.; Utt, A.; Ahola, T.; Kananovich, D. G.; Lopp, M.; Merits, A.; Karelson, M.; *Antimicrob. Agents Chemother.* **2016**, *60*, 7382.
58. Singh, H.; Mudgal, R.; Narwal, M.; Kaur, R.; Singh, V. A.; Malik, A.; Chaudhary, M.; Tomar, S.; *Biochimie* **2018**, *149*, 51.
59. Rashad, A. A.; Keller, P. A.; *J. Mol. Graphics Modell.* **2013**, *44*, 241.

Submitted: October 29, 2021

Published online: January 12, 2022

